Design considerations: From a Micro-Opto-Mechanical Pressure Sensor to a Micro-Opto-Mechanical Microphone

R. Haouari[1,2*], R. Jansen[2], V. Rochus[2], B. Figeys[1,2], L. Lagae[1,2] and X. Rottenberg[2]

[1] *Department of Physics and Astronomy*, KU Leuven,
Celestijnenlaan 200D, 3001 Heverlee, Belgium
[2]IMEC, *Kapeldreef 75, 3001 Heverlee, Belgium*

ABSTRACT

Microphones are dynamic pressure sensors specially dedicated to sound monitoring. In this paper, we analyse the design requirements for a micro-opto-mechanical pressure sensor (MOMPS) to work as an efficient micro-opto-mechanical microphone (MOMM) in the audio domain. These types of optical sensors are of interest for they can be operated in remote, harsh and sensitive environments. We further develop analytic formalism to investigate the bandwidth, dynamic range, sensitivity and signal-to-noise ratio (SNR) of MOMM devices. With the insight obtained, design considerations are then extracted and was applied to our MOMPS to make a MOMM.

Keywords: microphone, pressure sensor, optical sensor, Mach-Zehnder.

1 INTRODUCTION

Miniaturized microphones already achieve high accuracy, quality and sensitivity. These are typically implemented using electret condenser, piezoelectric micro-electromechanical systems (MEMS), piezoresistive MEMS [1] [2] technologies. However, the core function of those transducers relies on integrated electric circuits, what makes them sensitive to the environment they operate in. This leads typically to seal these devices in casings, thus impacting negatively their characteristics. Therefore, the perspective of using microphones in harsh or biological environments (e.g., underwater, inside a corrosive chamber, intracutaneous, biological tanks,…), leads us to consider the development of a novel family of devices that do not rely on integrated electrical readout.

Photonic systems present both a very good resistance to harsh environments and exhibit typically higher sensitivities than electrical ones. Previous work on MOMPS and MOMM hydrophones where already undertaken, mostly based on optical fibers [3]. In this paper, we extend our previous work on MOMPS using SiN waveguide technologies from a static to a dynamic description towards a MOMM function meeting speech receive specifications.

2 MOMPS WORKING PRINCIPLE

Optical interferometry is widely used for high resolution, highly sensitive measurements. It is recognized as one of the (if not the) techniques of choice for displacement, acceleration, ... measurements as it uses ultra-high frequencies and ultra-small wavelength as scales. A general interferometer splits a reference optical signal in two beams that travel through different paths, i.e., arms of the interferometer, before recombining. While the first arm acts as a reference, the other one undergoes a physical perturbation, representative of the quantity to measure, resulting in a change in its effective length. The optical phase difference introduced between the two arms translates at the output, after beam recombination, in an amplitude swing, direct measure for the quantity to be sensed.

The operation of the MOMPS in [4] is based on the Mach-Zehnder interferometry (MZI) principle. It consists of an input grating coupler, a multimode interferometer (MMI) splitter, two mainly spiraling waveguide arms, a MMI combiner and an output grating coupler (**Error! Reference source not found.**).

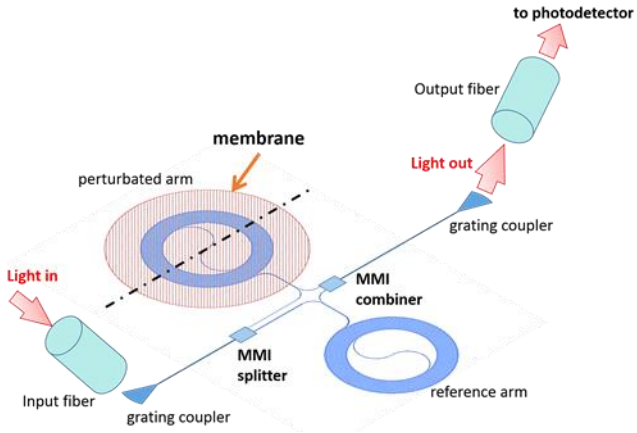

Figure 1. *Working principle of the designed MOMPS. A photonic circuit made of 2 grating couplers, MMIs and propagating waveguide form a Mach-Zehnder interferometer. The waveguide is defined as a long spiral path to amplify the strain that the membrane undergoes. Light couples in and out through grating couplers. The dotted line indicates the position of the cut plane shown in* ***Error! Reference source not found.****.*

Grating couplers allow to couple light in and out of our photonic circuit. Both arms present a same spiral as a waveguide path to obtain a balanced MZI (see **Error! Reference source not found.**). One of those spiral is defined

on a flexible membrane subjected to a pressure load while the other acts as a fixed reference. When the membrane bends, both the radial and azimuthal strain change the spiral length. Although the actual strain of the membrane can be small, the length of the spiral waveguide "amplifies" it. This leads to a time delay and phase difference between the signal coming out from both MZI arms, and hence, varying the output intensity emerging from the combiner. We measure it on a photodiode after the light coupled out through the other grating coupler. The position of the waveguide in the membrane thickness must be also considered. This MOMPs was manufactured with our proprietary SiN-based technology. The SiN core of the waveguides is 510 nm wide and 300nm high ensuring single modality at 850 nm wavelength. They are buried in an asymmetric silicon oxide (SiO) cladding so as to position the waveguides below the neutral axis of the membrane, i.e., bottom and top cladding are respectively 2.3 µm and 4.5 µm thick.

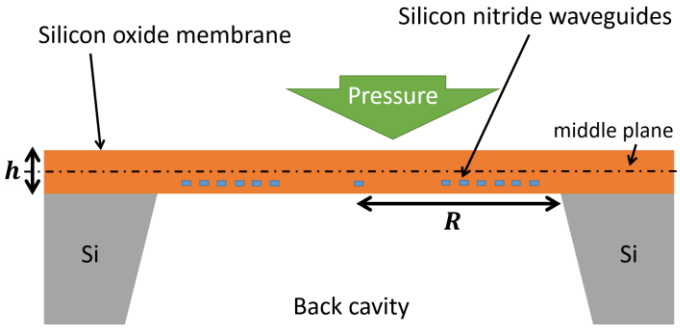

Figure 2. *Cross-section of the MOMPS along the dotted line in* ***Error! Reference source not found.****. In orange, the silicon oxide membrane hanging over a hole in the Si(grey) wafer; in blue, silicon nitride waveguides which present an offset regarding the middle neutral plane (dotted line).*

3 STATIC ANALYTICAL MODEL OF THE MOMPS

Large plate deflection model is used to describe the membrane with a radius R very large than its thickness h while undergoing a pressure p [5]. This model is correct for deflections up to a few times the thickness h. Derived from it, the deflection $w(r)$ of a clamped plate of a radius R can be put into the following form:

$$w(r) = w_0\left(1-\frac{r^2}{R^2}\right)^2 \quad (1)$$

where w_0 is the deflection at the centre and r represent the radial coordinate. For a plate of thickness h with the presence of a residual tensile strain ε_i, the expression of the central deflection is:

$$w_0 = \left(\frac{\beta}{2}+\gamma\right)^{1/3} + \left(\frac{\beta}{2}-\gamma\right)^{1/3} \quad \text{with}$$

$$\alpha = 14\frac{4h^2+3a^2\varepsilon_i(1+\nu)}{(1+\nu)(23-9\nu)}$$

$$\beta = \frac{7pR^4h^2}{8D(1+\nu)(23-9\nu)} \quad \gamma = \sqrt{\frac{\alpha^3}{27}+\frac{\beta^2}{4}} \quad (2)$$

In which we can find the flexural rigidity

$$D = \frac{E\,h^3}{12(1-\nu^2)} \quad (3)$$

depending on the Young's modulus E, the Poisson ratio ν and the thickness h. The deflection follows a cubic root evolution as a function of the pressure. After Taylor development analysis around p=0 we can find:

$$w_0 \approx \frac{R^4h^2}{16D\left(4h^2+3R^2\varepsilon_i(1+\nu)\right)}p \quad (4)$$

Using (1) and (3), it is possible to evaluate both the deformation and strain tensors of the plate, which lead us to the evaluation of the waveguide elongation ΔL:

$$\Delta L = \int_{waveguide}\varepsilon_s\,ds = \frac{4w_0z}{R}n_{spir}\,F_{geom} \quad (5)$$

with ε_s the local elongation of the waveguide along the spiral. The result of this integral is not explicated here but it is proportional to the product of the number of loops n_{spir} in our spiral and F_{geom}, an adimensional parameter linked to the length and the inner and outer radii of our spiral. Finally, the recombination of the two light gives a signal which vary in intensity due to the phase shift:

$$I_{out} = I_{in}\left(\cos\left(\pi\, n_{eff}\frac{\Delta L}{\lambda_0}\right)\right)^2 \quad (6)$$

with n_{eff} the effective mode index of the waveguide at λ_0, I_{in} the input power assuming no optical losses. Here it is assumed that changes in n_{eff} are negligible in comparison to the waveguide losses. The normalized output intensity I_{out}/I_{in} versus the applied pressure p is shown in **Error! Reference source not found.**. The quasi linear region in the first period gives the highest sensitivity. The inclusion of a $\pi/2$ phase shift between both MZI arms allows to shift that sensitive linear region to p=0. From equations (4) and (5) one can calculate the pressure range Δp_{range}, defined as the linear range with less than 1% error, and the maximal sensitivity S of the MOMPS:

$$\Delta p_{range} = \frac{\pi}{3K}$$

$$S_I = \frac{\partial I_{out}}{\partial p} = -I_{in}\frac{K}{2}$$

$$\text{with} \quad K = \frac{2\pi\, n_{eff}\, z\, n_{spir}\, F_{geom}\, R^3h^2}{\lambda D\left(4h^2+3R^2\varepsilon_i(1+\nu)\right)} \quad (7)$$

with z the distance of the waveguides from the middle plane of the plate.

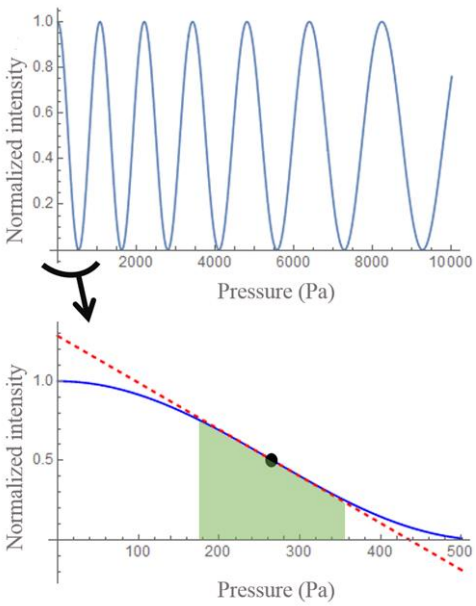

Figure 3 *Upper graph: Normalized evolution of the output intensity (regarding its maximum value) from the MMI combiner regarding the pressure. The cosine curve present an increasing pressure period. Bottom graph: zoom was made to have the first descending slope. The linear region was emphasized by plotting the tangent (red dashed line) around the operating point in black. The green indicates the linear region within 1%.*

4 FREQUENCY STUDY OF THE MOMPS

For the MOMS to work as a microphone with a broadband linear response it is crucial to make sure no membrane resonance occur within the bandwidth of the microphone. It is therefore sufficient to design the membrane such that the frequency of the fundamental axisymmetric resonance mode is beyond the bandwidth of the microphone. The fundamental resonance frequency of a clamped circular plate with radius R, thickness h and tensile stress N_0 is given by:

$$f_{00} = \frac{1}{2\pi R^2}\sqrt{\frac{D}{\rho h}}\ \gamma_{00}\sqrt{\gamma_{00}^2 + R^2\frac{N_0}{D}} \tag{8}$$

with ρ the volumic mass and γ_{00} first solution of the transcendent equation:

$$\gamma_{00} = A\,R$$

$$A^2 = \frac{\sqrt{N_0^2+4D\rho h\omega^2}-N_0}{2D} \quad \text{and} \quad B^2 = \frac{\sqrt{N_0^2+4D\rho h\omega^2}+N_0}{2D}$$

$$J_0(A\,R)\,I_0(B\,R) + J_0(A\,R)I_0(B\,R) = 0 \tag{9}$$

$J_0(r)$ and $I_0(r)$ denoting respectively the normal and modified Bessel functions of first kind.

At frequencies much smaller than f_{00}, the membrane can be described with the quasi-static model from previous section. Hence, the deflection due to an applied pressure and the dimensional parameters as described in (6) are still valid for the description of the microphone. This analytical description of the MOMPS will be used in the next section to find out which parameters are important/need to be altered in the future to design a performing microphone.

5 SPECIFICATIONS FITTING AND OPTIMIZATION TO A MOMM

In this paper we investigate the four main characteristics of a microphone: the bandwidth, the dynamic range, the sensitivity and the signal-to-noise ratio (SNR). A summary of the evolution of each microphone characteristic regarding the parameters is summarized in Table 2. We propose a set of values for those parameters in order to obtain a microphone for the audible spectrum.

The bandwidth of a microphone is defined as its frequency span up to its fundamental resonance. This can be computed with equation (7). Since we consider the spectrum from 300 Hz till 3.5 kHz, the fundamental frequency needs to be larger than the Nyquist frequency around 8 kHz.

The SNR of the MOMM is mainly governed by the technology platform in which we developed the MOMPS, the SNR of the laser, the detector and the read-out circuit. We catalogue and sum the losses for each component of the photonic circuit:

Part device	Loss
Grating couplers	-8 dB
MMI splitter/combiner	0.1 dB
PECVD SiN waveguides	1dB/cm

Table 1. Loss components

These losses are still open for improvement. The grating couplers could be replaced by more performant grating couplers or by butt-coupling, the MMI splitters could in theory be brought down to lossless components, and also for the waveguide losses there is still margin for improvement.

The noise equivalent power (NEP) of the detector in our setup is around $3.10^{-14}\ W/\sqrt{Hz}$. The minimal detectable power P_{min} is given by

$$P_{min} = NEP\sqrt{BW} \tag{10}$$

with BW the bandwidth of the microphone, i.e. ~10 kHz. Knowing the laser input power and using equations (5) and (3), we can make it correspond to an actual minimal measurable difference of pressure Δp_{min}. Typical values for speech is 10^{-2} Pa. Therefore, we will set our SNR to:

$$SNR = \frac{10^{-2}}{\Delta p_{min}} \tag{11}$$

PARAMETERS	Bandwidth	Dynamic range	Sensitivity	Signal-to-Noise ratio	Meeting requirement
Dimensional					
• radius R • thickness h	R^{-2} $h^{-1/2}$	$-R^{-3}$ $-h$	$-R^{3}$ h^{-1}	R^{-1} n.a.	1250 µm 6 µm
Material and technology					
• wavelength λ • loses L_{loses} • photodetector responsivity G • laser intensity I_{in}	n.a. n.a. n.a. n.a. n.a.	λ n.a. n.a. n.a.	λ^{-1} ${L_{loses}}^{-1}$ G I_{in}	λ^{-1}. ${L_{loses}}^{-1}$ G I_{in}	850 nm / 0.55 A/W 25 mW
Design					
• amount of spiral loop n_{spir} • geometry (outer-inner loop radii) F_{geom} • middle plan offset z	n.a. n.a. n.a.	${n_{spir}}^{-1}$ ${F_{geom}}^{-1}$ z^{-1}	n_{spir} F_{geom} z	n_{spir} F_{geom} z	20 1 µm

Table 2. Design specification summary. Power trend on how each design parameter (in the left column) impacts the microphone specification (above line). When no trend was extracted, n.a. (non-applicable) is mentioned.

The total sensitivity is proportional to the responsivity G of the detector and the loses L_{loses}:

$$S_{tot} = -I_{in}\, L_{loses}\, G\, \frac{K}{2} \tag{12}$$

And at last, the dynamic range of a microphone is the difference in a dB scale, of the highest pressure that it can handle over the floor noise level. The latest should be expressed as a sound pressure equivalent level. The maximum pressure is equal to half the pressure range (equation(6)) and the lowest is derived from the SNR.

In the last column of Table 2, we provide a set of values for the design parameters to have a flat wideband microphone with a resonance at 10 kHz. The expected sensitivity is computed to be 88 nA/mPa. We suppose no residual stress in our plate although it is not possible. Nevertheless, we can still predict the shift occurred because of it thanks to the equations presented in this paper. Since we are not planning to change the technology platform, optimization and evolution regarding the material parameters were not shown in Table 2.

6 CONCLUSION

We extended the static formalism describing the design and function of MOMPS to describe their dynamic behaviour and their use as MOMM for speech application. From this study, we conclude that those requirements can be met. Key parameters that impact greatly our MOMM are the radius and the thickness of the membrane along with the number of loops of our spiral. Nevertheless, other parameters also impact the performance of the devices for which we provide an extensive model, design and optimisation scheme. As a final conclusion, our analysis confirms that MOMMs are fully able to meet the specification considered for speech application.

REFERENCES

[1] P. R. Scheeper, A. G. van der Donk, W. Olthuis and P. Bergveld, "A review of silicon microphones," *Sensors and Actuators*, pp. 1-11, July 1994.

[2] Brüel & Kjaer, Microphone Handbook Vol 1 : Theory, 1996.

[3] T. Lim, Y. Zhou and Y. Lam, "Fiber optic acoustic hydrophone with double Mach–Zehnder interferometers for optical path length compensation," *Optics Communication*, vol. 159, pp. 301-308, 15 January 1999.

[4] J. Roelof, R. Veronique and R. Xavier, "MICRO-OPTO-MECHANICAL PRESSURE SENSOR (MOMPS) IN SIN INTEGRATED PHOTONICS PLATFORM".

[5] W. P. Eaton, F. Bitsie, J. H. Smith and D. W. Plummer, "A New Analytical Solution for Diaphragm Deflection and its Application to a Surface-Micromachined Pressure Sensor," in *International Conference on Modeling and Simulation of Microsystems*, 1999.

[6] B.Dong, "Nano-opto-mechanical (NOM) acoustic wavefront sensor via ring resonators," in *TRANSDUCERS EUROSENSORS XXVII*, 2013.

[7] Z. X., "A Nano-opto-mechanical pressure sensor," in *2011 16th International Solid-State Sensors, Actuators and Microsystems Conference*, 2011.

[8] Z. X., "A nano-opto-mechanical pressure sensor via ring resonator," *Opt. Express*, vol. 20, pp. 8535-8542, April 2012.

[9] Z. X., “Pressure sensor using Nano-opto-mechanical Systems (NOMS),” in *2011 16th International Solid-State Sensors, Actuators and Microsystems Conference*, 2011.

[10] H. Wu and S. Zhou, “Free vivrations of sensor diaphragm with residual stress coupled liquids,” *Journal of Applied Physics*, vol. 115, 2014.

[11] V. Rochus, J. Roelof, J. Goyvaert and X. Rottenberg, “Fast Analytical Model of MZI Micro-opto-Mechanical Pressure Sensor,” *Mechatronic Journal*, (in review).

[12] V. Rochus, R. Jansens, J. Goyvaert and X. Rottenberg, “Design of a MZI Micro-Opto-Mechanical Pressure Sensor for a SiN Photonics Platform,” in *IEEE Eurosime*, Montpellier, France, 2016.